Electron scattering on circular symmetric magnetic profiles in a two-dimensional electron gas

J. Reijniers, F. M. Peeters,* and A. Matulis†
Departement Natuurkunde, Universiteit Antwerpen (UIA), Universiteitsplein 1, B-2610 Antwerpen, Belgium
(Received 18 June 2001; published 3 December 2001)

Quasibound and scattered states in a two-dimensional electron gas (2DEG) subjected to a circular symmetric steplike magnetic profile with zero average magnetic field are studied. We calculate the effect of a random distribution of such identical profiles on the transport properties of a 2DEG. We show that a nonzero Hall resistance can be obtained, although $\langle B_z\rangle = 0$, and that in some cases it can even change sign as function of the Fermi energy or the magnetic-field strength. The Hall and magnetoresistance show pronounced resonances apart from the Landau states of the inner core, corresponding to the so-called quasibound snake orbit states.

DOI: 10.1103/PhysRevB.64.245314 PACS number(s): 73.40.−c, 73.20.−r, 73.50.Jt

I. INTRODUCTION

The response of a two-dimensional electron gas (2DEG) to a spatially inhomogeneous magnetic field has been the subject of considerable interest in recent years.[1] At very low temperatures and in very pure samples, these inhomogeneities in the magnetic field can act as scattering centers for the 2DEG, perturbing the ballistic electron motion and hence altering the transport properties of the 2DEG.

These inhomogeneous magnetic fields can be realized by growing a type-II superconducting film on top of a heterojunction, containing a 2DEG.[2] If a background magnetic field is applied, vortices will penetrate the 2DEG, where they form scattering centers. If the applied magnetic field is low, the vortices will be distributed randomly, due to the inhomogeneities in the superconducting film. Brey and Fertig[3] and Nielsen and Hedegård[4] studied scattering on these vortices if distributed randomly, and if distributed on a periodic array.

In an alternative approach superconducting particles are deposited above a 2DEG. Due to the Meissner effect, magnetic flux will be expelled from the particles, which again results in a low-magnetic-field region underneath each of the superconducting particles. This was realized by Smith *et al.*,[5] who grew lead grains on top of a heterojunction.

A logic next step would be to deposit ferromagnetic clusters as inhomogenous magnetic field creators in the 2DEG. This was realized by Ye *et al.*,[6] who grew Dy micromagnets on top of a GaAs/Al_xGa_{1-x}As heterostructure and recently by Dubonos *et al.*,[7] who studied scattering of electrons on the stray field of a single Dy magnet. This problem is essentially different from the earlier problems, because now the average magnetic-field strength is zero; $\langle B_z\rangle = 0$.

Preliminary results on this system were already presented in Refs. 8 and 9, where scattering on the stray fields of infinitesimally flat magnetic disks with perpendicular magnetization was studied. In this paper we extend and generalize these earlier results, and study cylindrical symmetric steplike profiles, with an average zero magnetic field. This simplification enables us to classify the arising phenomena and understand their underlying physics. We will show that such a system can give rise to a nonzero Hall resistance, even though $\langle B_z\rangle = 0$. Moreover, such a system can host quasibound states, similar to the ones studied by Kim *et al.*,[10] who theoretically investigated the electron states of a circular symmetric magnetic-field profile, consisting of two regions with different magnetic field strengths inside and outside a radius R. In contrast to the bound states found by Kim *et al.*, here the electron states are quasibound, because we consider magnetic profiles which are finite in extent.

We will model the magnetic field by

$$B(r<R_a)=B_a,$$
$$B(R_a<r<R_b)=B_b,$$
$$B(r>R_b)=0, \tag{1}$$

with $B_b=-B_a/[(R_b/R_a)^2-1]$ such that the condition $\langle B_z\rangle = 0$ is satisfied. This magnetic-field profile models the one of a perpendicularly magnetized ferromagnetic disk as ''felt'' by a 2DEG underneath the disk. As an example, in Fig. 1 we plot the magnetic-field profile (solid curve) resulting from a ferromagnet with radius R_a and thickness $d/R_a = 1$, grown a distance $h/R_a = 0.1$ above a 2DEG, as shown in the inset. The dotted curve represents the magnetic field according to our model, where we have chosen $R_b/R_a \approx 2.8$ to account for the shape of the profile. A cutoff at R_b is made in order to simplify the calculations. We believe that, in doing this, the physics is not altered.

The parameters (R_a, R_b, B_a, and B_b) depend on the specific properties of the ferromagnetic material (as extent,

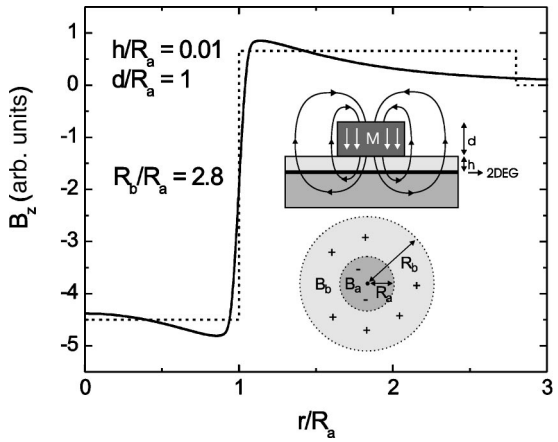

FIG. 1. The magnetic-field profile (solid curve) and the theoretical model (dotted curve) for a magnet of radius R and thickness $d/R = 1$, deposited a distance $h/R = 0.01$ above a 2DEG, as shown in the inset. The lower inset shows a simplified top view of the magnetic-field profile in the plane of the 2DEG.

thickness, magnetization, and distance to the 2DEG). The resulting profile can also be affected by including superconducting strips, which expel the flux lines due to the Meissner effect and consequently can rearrange or guide the magnetic field lines.

The paper is organized as follows. In Sec. II we consider scattering on a single magnetic profile. First we solve the problem classically in order to get a reference frame which describes the large energy limit. Then we concentrate on the quantum-mechanical behavior, and study the differences which arise, such as, e.g., the existence of quasibound states. In Sec. III, we calculate the response of the 2DEG to a random, homogeneous distribution of these (identical) profiles over the sample. The approach is along the lines presented by Nielsen and Hedegård in Ref. 4, which was based on the Boltzmann transport equation. Again, we consider the scattering both classically and quantum mechanically, and discuss the arising differences. In Sec. IV we summarize our conclusions, and briefly discuss the possibility of reproducing our results experimentally.

II. SCATTERING ON A SINGLE MAGNETIC PROFILE

A. Classical scattering

Classically, the scattering on a magnetic field profile is determined by the solution of Newton's equation of motion, where the force is given by the Lorentz expression $\mathbf{F}=e\mathbf{v}\times\mathbf{B}$ for a particle with charge e. Outside the profile, no magnetic field is present, and consequently the path is just a straight line. Inside the profile, the electron describes an arc of a circle, of which the radius (and the direction in which it is drawn, i.e., clockwise or counterclockwise) depends on its position in the profile, since the profile considered here consists of two regions with different magnetic-field strength (and sign). The respective cyclotron radii are given by $l_c=v/\omega_c$, where v is the velocity of the electron and $\omega_c=eB/mc$ is the cyclotron frequency in the local magnetic field, which is $B=B_a$ in the inner core and $B=B_b$ in the outer region.

The geometry of the scattering process is determined by the following dimensionless parameters: (a) R_b/R_a, i.e., the ratio of the radii of the inner and the outer circle of the magnetic field profile, and (b) $l_a/R_a=(m/e)(v/B_a)$, which is the ratio of the cyclotron radius in the inner core, to the radius of this center part. It is clear from geometrical considerations that it is impossible for a particle which was initially outside the magnetic profile to become trapped inside the magnetic profile.

We calculated the differential cross section $d\sigma/d\phi$ numerically, from the different classical trajectories. In Fig. 2, we show examples of the classical trajectories (on the right), and their resulting cross sections (bold curves, on the left) for the $R_b/R_a=1.5$ configuration for different l_a/R_a.

In the limit of $l_a/R_a\to 0$, the cyclotron radius is very small compared to R_b, and, therefore, the electron scatters on the magnetic profile as if it were bouncing off a hard wall. As a consequence, the differential cross section would be symmetric in ϕ. From Fig. 2, we see that if l_a/R_a increases, the differential cross section changes drastically, and loses its

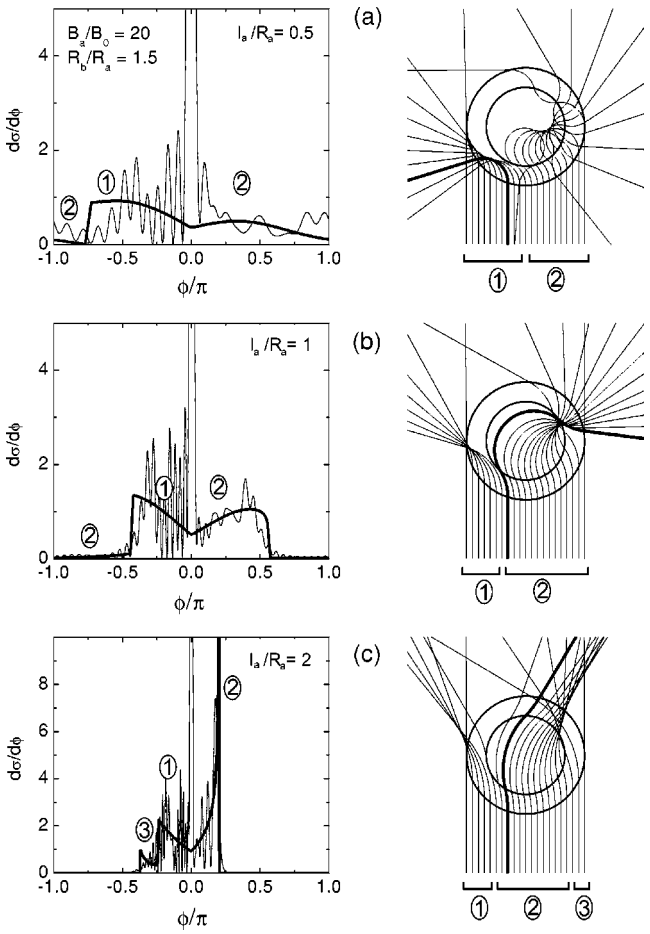

FIG. 2. This figure corresponds to the situation $B_a/B_0=20$ and $R_b/R_a=1.5$. On the left, the differential cross section for different $k/B_a=l_a/R_a$, i.e., (a) $l_a/R_a=0.5$, (b) $l_a/R_a=1$, and (c) for $l_a/R_a=2$. The bold curve corresponds to the classical result, and the thin curve to the quantum mechanical result. On the right, some classical trajectories interacting with the magnetic profile, resulting in the differential cross sections on the left. The trajectories giving rise to the different parts of the different structures, are grouped schematically.

symmetry due to the time-reversal-breaking magnetic field. We note that $d\sigma/d\phi$ is sensitive to l_a/R_a: for increasing l_a/R_a, it is more centered around 0, but its structure also changes significantly, which can be understood by inspection of the different classical electron trajectories shown on the right.

Suppose we consider the classical trajectories from left to right. In the case $l_a/R_a=0.5$, the electrons are deflected to the left ($\phi<0$), giving rise to the orbits indicated by (1), and contributing to the differential cross section indicated by (1). Shifting the initial position of the electron further to the right, at a certain point the electron does not only feel the outer region, but is able to penetrate into the inner core; consequently the electron is abruptly swept to the other side. The latter causes the abrupt decrease of $d\sigma/d\phi$ at $\phi/\pi=-0.75$. These trajectories contribute to part (2) in the differential cross section, and have mainly $\phi>0$.

The same reasoning can be used to understand the differential cross section for $l_a/R_a=1$; only now, $d\sigma/d\varphi$ is more

centered around zero due to the higher velocity of the electron (with respect to the magnetic field), i.e., the electron is less deflected. For larger velocities, e.g., for $l_a/R_a=2$ as in Fig. 2(c), the previous picture has to be extended with a new type of trajectories: those on the right (3) which again only probe the outer region, since the magnetic field in the outer region is not strong enough to deflect the electron into the inner part. These trajectories give rise to an additional peak (3) in the differential cross section.

B. Quantum-mechanical scattering

1. Schrödinger equation

We have to solve the Schrödinger equation

$$(H-E)\Psi(r,\varphi)=0, \tag{2}$$

where $E=\hbar^2k^2/2m$ is the energy of the scattering wave. Because of cylindrical symmetry, we work with polar coordinates $\mathbf{r}=(r,\varphi)$. We can make this equation dimensionless by rescaling the problem in the following way: length $R_0=R_a$, energy $E_0=\hbar^2/(mR_a^2)$, time $t_0=mR_a^2/\hbar$, and magnetic field $B_0=c\hbar/eR_a^2$. We can write the scattering wave function as consisting of components, separated into an angular and radial part,

$$\Psi(r,\varphi)=\sum_{m=-\infty}^{\infty} R_{km}(r)\Phi_m(\varphi), \tag{3}$$

for which the angular part is equal to

$$\Phi_m(\varphi)=\frac{1}{\sqrt{2\pi}}e^{im\varphi}, \tag{4}$$

since the problem is cylindrically symmetric. The Schrödinger equation is then reduced to only one dimension,

$$\left[-\frac{1}{2r}\frac{d}{dr}r\frac{d}{dr}+V_m(r)-E\right]R_{km}(r)=0, \tag{5}$$

with

$$V_m(r)=\frac{1}{2}\left[A_\phi(r)+\frac{m}{r}\right]^2, \tag{6}$$

the effective potential, and $A_\phi(r)=(1/r)\int_0^r dr' r' B(r')$, the angular component of the vector potential. Note that the angular quantum number satisfies $-\infty<m<\infty$, in contrast to when the scatterers are nonmagnetic, in which case we have $0\leqslant m<\infty$, due to symmetry, i.e., m and $-m$ result in the same scattered wave.

We know that the scattering process is fully determined if we know δ_m for every m. In order to calculate these phase shifts, we have to solve Eq. (5) for every m in the presence of our magnetic profile, and compare the scattered wave with the unperturbed wave. The solution for $r<R_a$ is

$$R_{km}(r)=r^{|m|}e^{-1/2\,B_a r^2}c_{m,1}M(\alpha,\beta,\gamma), \tag{7}$$

and, for $R_a<r<R_b$,

$$R_{km}(r)=r^{|m|}e^{-1/2\,B_a r^2}[c_{m,2}M(\alpha',\beta,\gamma') + c_{m,3}U(\alpha',\beta,\gamma')], \tag{8}$$

where $M(a,b,c)$ and $U(a,b,c)$ are confluent hypergeometric functions,[11] $c_{m,1}$ is a normalization constant, $\alpha=[|m|+1-m-k^2/(2B_a)]/2$, $\beta=|m|+1$ and $\gamma=B_a r^2$. α' and γ' are the same as α and β, but with $B_a\rightarrow B_b$. The constants $c_{m,2}$ and $c_{m,3}$ have to be determined such that the wave function is continuous at $r=R_a$. An alternative approach is to calculate the wave function numerically up to $r=R_b$.

For $r>R_b$, Eq. (5) reduces to

$$\left[-\frac{1}{2r}\frac{d}{dr}r\frac{d}{dr}+\frac{m^2}{2r^2}-\frac{k^2}{2}\right]R_{km}(r)=0, \tag{9}$$

which is the differential equation for the Bessel function of the first kind:

$$R_{km}(r)=a_m J_m(kr)+b_m Y_m(kr). \tag{10}$$

Therefore, the resulting phase shifts can be calculated at this point, $r=R_b$, and are derived from the condition that the logarithmic derivative of the radial wave function must be continuous at this boundary,

$$\left.\frac{1}{R_{km}^<}\frac{dR_{km}^<}{dr}\right|_{r=R_b}=\left.\frac{1}{R_{km}^>}\frac{dR_{km}^>}{dr}\right|_{r=R_b}\equiv\xi_{km}, \tag{11}$$

which results in

$$\left.\frac{1}{R_{km}^<}\frac{dR_{km}^<}{dr}\right|_{r=R_b}=\frac{j_m(kR_b)-y_m(kR_b)\tan\delta_m}{J_m(kR_b)-Y_m(kR_b)\tan\delta_m}, \tag{12}$$

where we have introduced the abbreviations $z_m(x)=(x/2)[Z_{m-1}(x)-Z_{m+1}(x)]$ with $(z,Z)=(j,J)$ or (y,Y). It is now easy to solve for δ_m:

$$\tan\delta_m=\frac{j_m(kR_b)-\xi_{km}J_m(kR_b)}{y_m(kR_b)-\xi_{km}Y_m(kR_b)}. \tag{13}$$

2. Resonances

In contrast to the classical problem, the ratio l_a/R_a no longer determines the scattering problem completely. We need to know the exact energy and the magnetic-field strength, and therefore l_a/R_a should be extended with the exact E or B_a. We have chosen to fix the magnetic field strength $B_a/B_0=20$, and to plot all curves as a function of $k/B_a(R_aB_0)=l_a/R_a$, as was done in the classical case. The larger the k value ($\sim l_a/R_a$ for fixed B_a), the more classical the system is, and the more the average of it converges to our previously obtained classical result (see the thin solid curves in the right part of Fig. 2). But for lower k values, i.e., when the wavelength of the scattering wave is comparable to the dimensions of the scatterer $1/k\approx R_b$, quantum mechanics becomes important, and results in features which cannot be understood classically, as e.g., the existence of resonances.

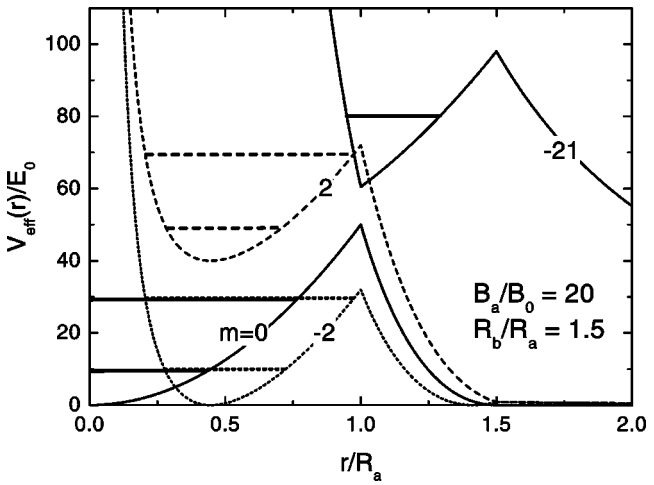

FIG. 3. The effective potential $V_{eff}(r)$ as function of r/R_a for various m values, for the case when $B_a/B_0=20$ and $R_b/R_a=1.5$. The horizontal lines correspond to the resonant energies.

In order to determine at which energies these resonances occur, one should inspect the phase shift δ_m as a function of the energy or the corresponding k vector. When a jump of π occurs, there is a resonance for that particular k value for given m. The lifetime of that quasibound state depends on the energy interval over which this jump occurs, or on the peak width of the partial cross section σ_m as a function of the energy.

In the following, we show the results for the case $B_a/B_0=20$ and $R_b/R_a=1.5$. In Fig. 3 we plot the effective potential for four different m values for this case. In Fig. 4 we plot the phase shift as a function of k/B_a for $-10\leqslant m \leqslant 10$.

We note that for $m\geqslant -2$ well-defined quasibound states are formed at the Landau levels of the inner core of the magnetic-field profile, i.e., at $k=\sqrt{B_a(2n+1)}=4.471$, 7.745, 10, . . . , or in the units of Fig. 4: $k/B_a=0.224$, 0.387, 0.5, ... Landau states in the outer region ($B_b/B_0=16$) are

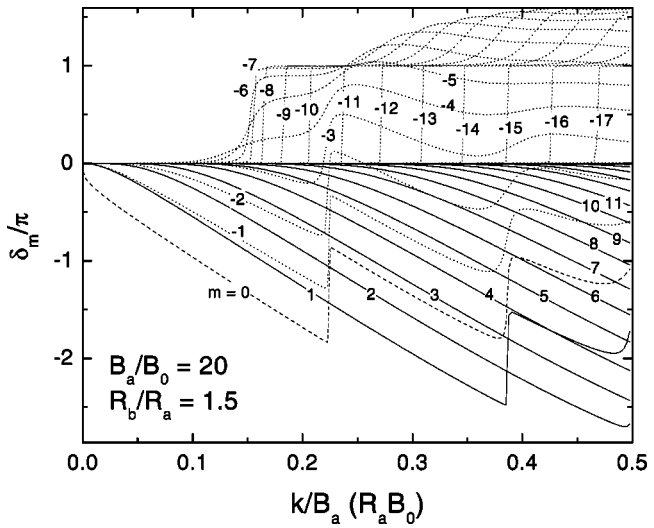

FIG. 4. The phase shift δ_m as a function of k/B_a for different m values, for the situation with $B_a/B_0=20$ and $R_b/R_a=1.5$. Phase jumps of π correspond to resonant states.

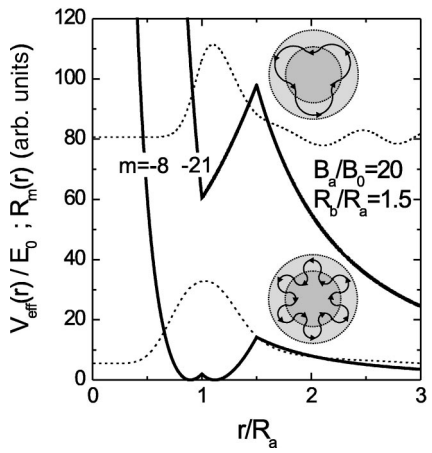

FIG. 5. The effective potential $V_{eff}(r)$ as function of r/R_0 for $m=-8$ and $m=-21$ when $B_a/B_0=20$ and $R_b/R_a=1.5$, together with the radial wave functions (dotted curves) at the resonant energies. These quasibound states correspond to different types of snake orbits, propagating parallel to the magnetic edge, as depicted schematically in the inset of the figure.

not possible since the total extent of the lowest Landau state ($=2l_b=2R_a/\sqrt{20}=0.5R_a$) does not fit into the outer region ($R_b-R_a=0.5R_a$).

Nevertheless, for $m<-4$ there are also resonances which have an energy lower than the first Landau level of the inner core. They correspond to quasibound snake orbit states, which travel around the profile, propagating from the B_a region into the B_b region, and vice versa. As an example we plot the effective potential and the corresponding radial wave function R_m for $m=-8$ in Fig. 5. Because the two wells, corresponding to the magnetic confinement in the different magnetic fields of the inner and outer regions, are joined together, they form one well which is broader—and consequently has an energy lower—than each of the separate wells. A similar effect we encountered in a previous paper for the case of electron traveling along a one-dimensional magnetic interface.[12] The electrons propagate classically, as schematically depicted in the inset of Fig. 5.

For higher energies we also note resonances for negative m, e.g., for $m=-21$, as shown in Fig. 5. They too correspond to snake orbits, but, because they have a larger energy they have to move closer to the interface, in order not to escape the magnetic-field profile, since their cyclotron radius is larger. These type of states become extinct when the cyclotron radius in the outer part exceeds the radius of the outer part R_b, i.e., for $kl_a\approx R_b/R_a=1.5$. We have checked this, and these resonances indeed disappear.

3. Differential cross section

In two dimensions, the differential cross section is given by

$$\frac{d\sigma}{d\phi}=\frac{2}{\pi k}\left|\sum_{m=-\infty}^{\infty} e^{im\varphi}e^{-i\delta_m}\sin\delta_m\right|^2. \qquad (14)$$

We plot this together with its classical counterpart in Figs. 2(a)–2(c). We note that many oscillations are present, due to

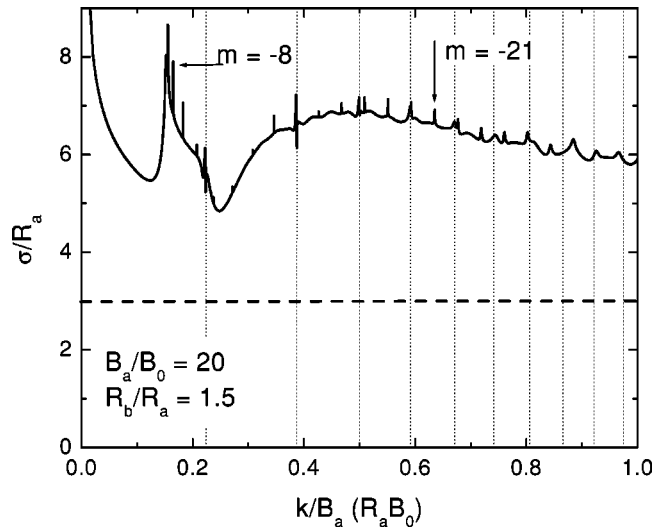

FIG. 6. The cross section σ as a function of k/B_a in the classical limit (dashed curve) and if calculated quantum mechanically (solid curve) for $B_a/B_0=20$ and $R_b/R_a=1.5$. The marked resonant states correspond to the ones shown in Figs. 5 and 8. Vertical dotted lines are the Landau energies of the inner core of the magnetic-field profile.

interference effects. The number of these oscillations depends on the energy: the larger the energy, the greater the number of oscillations. In the high-energy limit, the quantum-mechanical result will ultimately, on the average, converge to the classical one, except for the peak at $\phi=0$. Its occurrence is a purely quantum-mechanical effect, and is due to the fact that an electron which would classically pass by—and hence does not interact with—the scatterer, quantum mechanically, has a finite overlap with the scatterer, and consequently contributes—although very little—to the cross section. Because the interaction is very slight, it is only scattered over a very small angle, and thus adds to the $\phi=0$ peak.

4. Total cross section

In Fig. 6 we plot the total cross section $\sigma=\int d\phi d\sigma/d\phi$ as a function of k/B_a. Classically, this is equal to the total diameter of the magnetic inhomogeneity $\sigma=2R_b$ (dashed line in Fig. 6). From Fig. 6 we note that the quantum-mechanical cross section (solid curve) is larger than the classical result. For large energies the total cross section is twice as large; for small energies the cross section is four times as large, as is the case for scattering on a spherical hard wall. We also note the resonances mentioned before, present as small peaks, which can be attributed to a particular m value. As an example, we indicated the $m=-8$ and -21 resonances, corresponding to the quasibound states of Fig. 5.

III. SCATTERING ON MULTIPLE PROFILES

With a knowledge of the classical and quantum-mechanical differential cross sections, it is now possible to calculate the Hall and magnetoresistance in a 2DEG subjected to a randomly distributed array of such identical profiles. We will make the assumption that the dimensions of the magnetic disks are small compared to the distance between the disks, so we do not include interference effects between different scattering events. Moreover, we neglect impurity scattering.

We solve the (classical) Boltzmann transport equation, linearized in the electric field, and follow the derivation as described in the paper of Nielsen and Hedegård.[4] Finally, we arrive at

$$\rho_{xx}=\frac{1}{(2\pi)^2}\frac{n_0}{n_e}\frac{\hbar}{e^2}\int_{-\pi}^{\pi}d\phi(1-\cos\phi)w(k,\phi), \quad (15a)$$

$$\rho_{xy}=\frac{1}{(2\pi)^2}\frac{n_0}{n_e}\frac{\hbar}{e^2}\int_{-\pi}^{\pi}d\phi\sin\phi w(k,\phi), \quad (15b)$$

where n_e is the electron concentration, n_0 is the concentration of magnetic scatterers, and $w(k,\phi)$ is the probability for an electron with wave vector k to be scattered over an angle ϕ. In relation to the differential cross section, we can write $w(k,\phi)=(\hbar k/m)(d\sigma/d\phi)$, since $\sigma v\Delta t$ is the probability for an electron with velocity v to interact with a scatterer with cross section σ in a time interval Δt.

A. Classical result

1. Magnetoresistance

In Fig. 7(a), we plot the magnetoresistance as a function of l_a/R_a for various R_b/R_a, in units of $\rho_0=(n_0/n_e)(\hbar/e^2)$. This is obtained by inserting the earlier calculated classical $d\sigma/d\phi$ into $w(k,\phi)$ of Eq. (15a). The magnetoresistance is zero when $l_a/R_a=0$, because, for zero energy, electrons do not move ($v=0$), and consequently do not experience any scattering. For small values the magnetoresistance increases linearly up to a certain value, after which it decreases for increasing l_a/R_a. This decrease is due to the fact that for higher energy, the electrons are less deflected because of a larger cyclotron radius in the magnetic inhomogeneity. We note that for increasing R_b/R_a the magnetoresistance has an overall increase, which can be explained by considering scattering on the inner and outer profiles and how they influence each other. For larger R_b/R_a, the cyclotron radius of the outer part increases quadratically in R_b/R_a; therefore, electrons will be less deflected for increasing R_b/R_a. However, this is compensated for by the fact that the cross section also increases linearly with R_b/R_a, and consequently scattering on the outer part has more or less the same impact for different R_b/R_a. Therefore, the increase in the resistance is due to the fact that for larger R_b/R_a, the scattering on the inner and outer regions can be considered as two separate processes, which interfere with each other very little. This is not the case for smaller R_b/R_a, where electrons interacting with the outer part are more likely also to interact with the inner part, which would deflect the electron in the opposite way, and thus diminishes the scattering effect produced by the outer part. In short we can say that electrons, which interact with the magnetic profile,

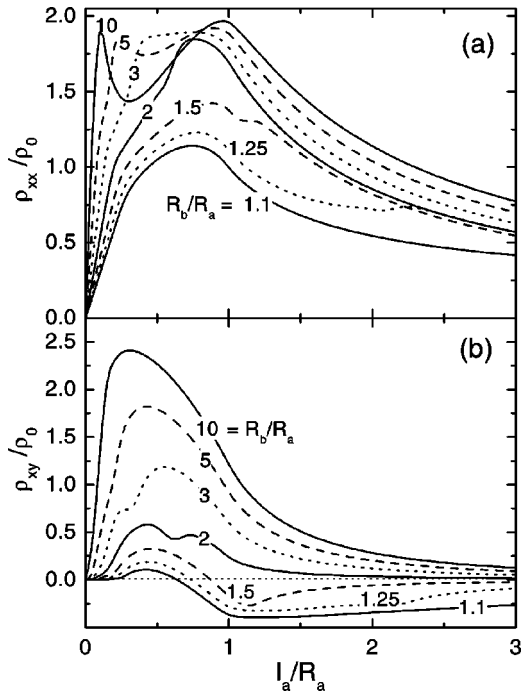

FIG. 7. The magnetoresistance (a) and the Hall resistance (b) in the classical limit as a function of l_a/R_a for different R_b/R_a configurations.

on average ''feel'' a nonzero magnetic field which increases with increasing R_b/R_a, and this results in an increase of the magnetoresistance and the Hall resistance.

The fact that for higher R_b/R_a the scattering problem can be seen as two separate scattering processes on different vortices (R_a,B_a) and (R_b,B_b), is also reflected in the dip in the magnetoresistance which arises for higher R_b/R_a, e.g., $R_b/R_a=10$. Actually, the magnetoresistance has two peaks of which one, the lower-energy peak, corresponds to scattering on the outer region, while the second peak corresponds to scattering on the center region. For higher R_b/R_a, the first peak will shift toward smaller l_a/R_a, while the other peak remains in the same position; consequently, the two scattering processes will become more distinct.

2. Hall resistance

The corresponding Hall resistance is plotted in Fig. 7(b). We note that both qualitative and quantitative behaviors are more sensitive to the ratio R_b/R_a than was the case for the magnetoresistance. There are two striking features: (a) again, there is an overall increase of the Hall resistance with increasing R_b/R_a; and (b) for small R_b/R_a, i.e., $R_b/R_a<1.73$, the Hall resistance can change sign as a function of l_a/R_a, i.e., as a function of the Fermi energy or the magnetic-field strength.

The fact that the Hall resistance can change sign when $R_b/R_a<1.73$ is a consequence of the interplay between scattering in the inner and outer regions of the magnetic-field profile. For infinitesimally small l_a/R_a, the outer part will act as a hard wall, and consequently there is no Hall resistance. For increasing l_a/R_a, the electrons will penetrate deeper in the outer region, but not yet in the inner core as long as l_a/R_a is small enough, i.e., $2l_b<(R_b-R_a)$ [see the trajectory given by the bold curve in the right figure of Figs. 2(a)]. The Hall resistance is due to a vortex with magnetic strength B_b. For increasing k/B_a, the electrons will be able to penetrate into the inner region, where they are deflected to the other side; consequently, the Hall resistance changes sign [see the bold curve in Figs. 2(b) and 2(c)].

The reason that this effect does not occur for higher R_b/R_a values is due to the fact that, in these cases, there is only little interplay between scattering in the inner and outer regions, as mentioned above. It is much more unlikely that an electron which initially only felt the outer region, for higher l_a/R_a, will interact with the (relatively small) core, and be swept to the other side. Therefore, the Hall resistance for large R_b/R_a always has the same sign, as generated by the outer region.

B. Quantum-mechanical result

After insertion of Eq. (14) into Eqs. (15a) and (15b), we can rewrite the magnetoresistance and the Hall resistance as functions of the phase shifts:

$$\rho_{xx}=\frac{n_0}{n_e}\frac{\hbar}{e^2}\sum_{m=-\infty}^{\infty}2\sin^2(\delta_m-\delta_{m+1}), \tag{16a}$$

$$\rho_{xy}=\frac{n_0}{n_e}\frac{\hbar}{e^2}\sum_{m=-\infty}^{\infty}\sin[2(\delta_m-\delta_{m+1})]. \tag{16b}$$

In Fig. 8, we plot the Hall resistance and the magnetoresistance as functions of k/B_a for $B_a/B_0=20$ and $R_b/R_a=1.5$. The solid curve is the quantum-mechanical result, and the dashed curve is our previously obtained classical result. We observe many resonances, which diminish for increasing k/B_a. Except for this, on the average there is rather good agreement between both curves, which is due to the choice of B_a/B_0 being large; consequently, in this figure k—and consequently the energy—is large.

There are two types of resonances: (1) those which occur at the energy of the Landau levels of the inner core of the magnetic-field profile (thin dotted curves), and (2) those corresponding to quasibound snake orbit states.

In case of the first type of resonance, the Hall resistance decreases abruptly (i.e., it has a sawtooth behavior), while the magnetoresistance increases. This can be viewed in the right inset in Fig. 8. The reason for this is that at the energy of the Landau levels (indicated by the vertical dotted lines), electrons are (quasi) bound into cyclotron orbits, and hence cannot (a) contribute to the conduction, and consequently the magnetoresistance increases; and (b) cannot pile up and generate a voltage difference on the left and right side, and consequently the Hall resistance decreases. Moreover, spending time circling around underneath the disk, the electron loses knowledge of where it came from. As a result, if the electron

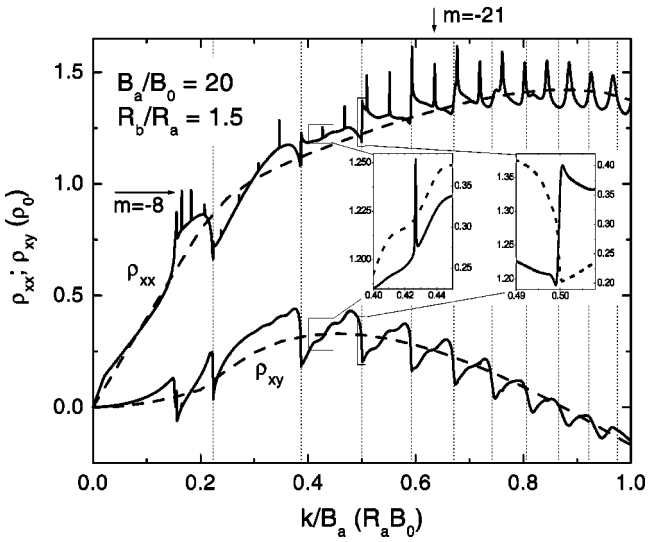

FIG. 8. The magnetoresistance and Hall resistance as functions of k/B_a in the classical limit (dashed curves) and if calculated quantum mechanically (solid curves) for $B_a/B_0=20$ and $R_b/R_a=1.5$. The marked resonant states correspond to the ones shown in Figs. 5 and 6, and the vertical dotted lines are the Landau energies of the inner core of the magnetic-field profile. The insets show enlargements of a quasibound snake orbit resonance (left) and a Landau-level resonance (right) where the solid curve corresponds to ρ_{xx} and the dashed curve to ρ_{xy}.

relaxes and escapes the scattering region, its chances to be scattered in the backward direction increase, and consequently the magnetoresistance also increases. The Hall resistance is a measure of the asymmetry of the scattering process, and we can therefore interpret the dips in ρ_{xy} along the same line of reasoning.

For larger energies, the cyclotron orbit in the center will increase and exceed the inner core classically at $k/B_a=1/(R_aB_0)$. Nevertheless, quantum mechanically the electron will ''feel'' the presence of the outer magnetic field, and this will change the resonant energies. The resistance jumps are also less explicit for higher Landau levels, which is due to the reduced number of states which fit in the core as a result of the large cyclotron radius.

Apart from resonant states at the Landau levels, the magnetoresistance exhibits very sharp peaks, which correspond to the snake orbit states mentioned earlier. This second type of resonances can have a lower energy than the first Landau level of both the inner and outer parts, as explained above. Since for all the snake orbit resonances only one quasibound state is involved (in contrast to the Landau states, where various quasibound states exist for various m values; see Figs. 3 and 4), these peaks are very sharp (see, e.g., the left inset of Fig. 8) and are superimposed on a more continuous background.

The influence of the quasibound snake orbit states is also visible in the Hall resistance, but not as pronounced as in the magnetoresistance. These quasibound states produce small changes in the slope of the Hall resistance ρ_{xy}, as is clear from the dashed curve in the left inset of Fig. 8.

IV. CONCLUSIONS

In this paper we studied scattering on circular symmetric magnetic-field profiles with zero mean magnetic field in the 2DEG. We considered scattering on a single profile, both classically and quantum mechanically, and found different types of quasibound states: the Landau states in the inner core, and different quasibound snake orbit states. Next we investigated the diagonal and Hall resistivities in the presence of a randomly distributed array of these magnetic profiles, using the kinetic Boltzmann equation, for different magnetic-field configurations. We obtained a nonzero Hall resistance although $\langle B_z\rangle=0$, and showed that the Hall resistance can change sign as a function of the Fermi-energy or the magnetic-field strength. We found that the electron resonances in the individual magnetic-field profiles are reflected in the Hall resistance and the magnetoresistance.

Considering a realistic magnetic-field profile as in the experiment will only rearrange or shift the positions of the resonances, but we expect no qualitative changes in our results. Note that similar resonances in ρ_{xx} and ρ_{xy} are expected to occur for composite fermions at the magnetic filling factor $\nu=1/2$. Nevertheless, measuring these resonances will be hard, since there are two competing effects which make an experimental measurement of these resonances difficult: in order to detect these quasibound states, it is necessary that the energies (bound or resonant) not be too close to each other. To obtain this, one has to make a very small magnet (since $E_0=\hbar^2/mR_a^2$), but then one encounters the problem that in order to bind the electrons in such a small area one needs a very strong inhomogeneous magnetic field ($B_0=c\hbar/eR_a^2$); currently no magnetic materials are available which can realize these strong fields.

An example of such a system is the one by Dubonos *et al.*[7]: they managed to deposit a single Dy magnet with a radius ≈ 0.1 μm on top of a heterojunction containing a 2DEG. For this system, our units are given by $E_0=7.63\times10^{-3}$ meV and $B_0=0.066$ T. The Fermi energy in their system was about $E_F=17.86$ meV, which in our units is $E_F=2341E_0$ or $k_F\approx 70$. According to Ref. 7 the stray field could locally generate magnetic fields of $B_a\approx 1T\approx 15B_0$, which corresponds to $k_F/B_a\approx 4.7$, for which we are in the classical regime and the scattering process can be calculated classically. In order to measure individual snake orbits, it is therefore necessary to include additional electrical confinement, which discretizes the energies and makes measurement possible, as also used in the paper by Nogaret *et al.*[13]

ACKNOWLEDGMENTS

This work was partially supported by the Inter-university Micro-Electronics Center (IMEC, Leuven), the Flemish Science Foundation (FWO-VI), the Belgian Interuniversity Attraction Poles (IUAP) and the Flemish Concerted Action (GOA) Programmes. J. R. was supported by ''het Vlaams Instituut voor de bevordering van het Wetenschappelijk & Technologisch Onderzoek in de Industrie'' (IWT).

*Email address: peeters@uia.ua.ac.be
†Email address: matulis@pub.osf.lt Permanent address: Semiconductor Physics Institute, Goštauto 11, 2600 Vilnius, Lithuania.

[1] F. M. Peeters and J. De Boeck, in *Handbook of Nanostructured Materials and Technology*, edited by N. S. Nalwa (Academic Press, New York, 1999), p. 345.
[2] A. K. Geim, Pis'ma Zh. Eksp. Teor. Fiz. **50**l, 359 (1989) [JETP Lett. **50**, 389 (1989)].
[3] L. Brey and H. A. Fertig, Phys. Rev. B **47**, 15 961 (1993).
[4] M. Nielsen and P. Hedegård, Phys. Rev. B **51**, 7679 (1995).
[5] A. Smith, R. Taboryski, L. T. Hansen, C. B. Sørensen, P. Hedegård, and P. E. Lindelof, Phys. Rev. B **50**, 14 726 (1994).
[6] P. D. Ye, D. Weiss, G. Luthering, R. R. Gerhardts, K. Von Klitzing, K. Eberl, H. Nickel, and G. Weimann, in *Proceedings of the 23rd International Conference on the Physics of Semiconductors* (World Scientific, Singapore, 1997), p. 1529.
[7] S. V. Dubonos, A. K. Geim, K. S. Novoselov, J. G. S. Lok, J. C. Maan, and M. Henini, Physica E **6**, 746 (2000).
[8] F. M. Peeters, A. Matulis, and I. S. Ibrahim, Physica B **227**, 131 (1996).
[9] J. Reijniers A. Matulis, and F. M. Peeters, Physica E **6**, 759 (2000).
[10] N. Kim, G. Ihm, H. S. Sim, and T. W. Kang, Phys. Rev. B **63**, 235317 (2001).
[11] *Handbook of Mathematical Functions*, M. Abramowitz and I. A. Stegun (Dover, New York, 1970), p. 504.
[12] J. Reijniers and F. M. Peeters, J. Phys.: Condens. Matter **12**, 9771 (2000).
[13] A. Nogaret, S. J. Bending, and M. Henini, Phys. Rev. Lett. **84**, 2231 (2000); J. Reijniers and F. M. Peeters, Phys. Rev. B **63**, 165317 (2001).